SCIENCE CHINA Materials ARTICLES

mater.scichina.com link.springer.com

Published online 27 November 2017 | https://doi.org/10.1007/s40843-017-9135-y

Sci China Mater 2018, 61(1): 101–111

Atypical $BiOCl/Bi_2S_3$ hetero-structures exhibiting remarkable photo-catalyst response

Muhammad Tanveer[1,2,3], Yu Wu[1], Muhammad Abdul Qadeer[4] and Chuanbao Cao[1*]

ABSTRACT **We demonstrate the fabrication of $BiOCl/Bi_2S_3$ which is well defined at a large scale. The $BiOCl/Bi_2S_3$ hetero-structures exhibit an enhanced photo-catalytic degradation of methyl orange (MO) compared to BiOCl and Bi_2S_3, attributed to the interface between Bi_2S_3 and BiOCl, which effectively separate the photo-induced electron-hole pairs and suppress their recombination.**

Keywords: bismuth sulfide, hetero-structures, photo-catalyst response

INTRODUCTION

A well-defined shapes at a large scale along with the alignment of nanobuilding blocks into well-ordered structures have been a key issue in modern colloid, material chemistry. The shape- and structure-dependent effects could develop, widespread and versatile potential applications. So, the morphological and structural tailoring of nano-/micro-crystals has emerged as an challenge [1–3]. Recently, hollow nanostructures, core-shell nanostructures and hetero-structures as a kind of new nano-/micro-structures have received an intense attention because of their improved physical and chemical properties over their single components [4–15].

In recent years, many attentions have been paid toward the general approach for preparing unusual and complex structures for versatile applications through the sacrificial templates including hard and soft templates [16–18]. However, the atypical architectures fabricated from hard template and through two-step synthetic strategies mostly suffering from their high cost and tedious synthetic procedures [19–25]. So it is highly desirable to develop one-pot synthesis of novel inorganic materials without templates and to explore their multifunction.

Moreover, for solar energy conversion, environmental purification and photo-catalytic technology, TiO_2, because of its excellent photocatalytic activities, low cost, chemical stability and environmental friendliness, has been promising semi-conductor photo-catalyst. But less utilization of solar energy on TiO_2 limits its extensive applications [26,27]. The exploitation of efficiently visible-light-driven photo-catalysts is essential and urgent for the practical application of photocatalytic technology. Two major approaches have been employed to extend the light absorption of semi-conductor photocatalysts to visible spectral region. The first one is the modification of TiO_2 through metals or non-metal doping and semiconductor coupling [28,29]. The second strategy is to exploit novel non-TiO_2-based semiconductor photocatalysts displaying strong visible light response. Among non-TiO_2-based semiconductors, emerging candidates to the exploit novel of photocatalyst in the visible region include Bi_2WO_6 [30], BiOCl, BiOBr [31–33], $InNbO_4$ [34] and $BiVO_4$ [35]. However, these strategies are expected to satisfy the large-scale application under visible light irradiation. Hence, the visible light activated photo-catalysts with high efficiency need to be fully investigated.

Recently, as a new type of non-TiO_2-based semiconductor photocatalyst with layered structure, high activity and high photocorrosion endurance, bismuth-based nanostructures have great attention for highly active photocatalysts under UV and visible light illumination [36]. Among all of these photo-catalysts, BiOCl, composed of $[Bi_2O_2]^{2+}$ layers interleaved with Cl double layers,

[1] Research Centre of Materials Science, Beijing Key Laboratory of Construction Tailorable Advanced Functional Materials and Green Applications, Beijing Institute of Technology, Beijing 100081, China
[2] Department of Physics, School of Physical Sciences, University of the Punjab, Lahore, Pakistan
[3] Department of Physics, University of Lahore (UOL) (Gujrat Campus), Gujrat, Pakistan
[4] Key Laboratory for Green Chemical Technology of the Ministry of Education, School of Chemical Engineering and Technology, Tianjin University, Tianjin 300072, China
* Corresponding author (email: cbcao@bit.edu.cn)

has been reported to be an important photocatalyst for degradation of various organic compounds under UV light illumination [37]. However, its photocatalytic activity has also been limited by its wide band gap and high recombination of photo-generated electron-hole pairs. Chang *et al.* [38] coupled BiOCl with a narrow band gap material, $NaBiO_3$. Moreover, BiOCl nanoparticles were dispersed uniformly on the both surfaces of graphene sheets to form a sandwich-like structure. The graphene/BiOCl nanocomposite increased the separation efficiency of electron-hole pairs and enhanced photo-degradation of methylbenzene under irradiation [39]. Very recently, $BiOCl/Bi_2S_3$ hetero-structures have been fabricated through ion exchange strategies and a degradation of methyl orange, RhB and 2,4-dichlorophenol (2,4-DCP) has been carried out under the visible light irradiation. In all of these two-step synthetic approaches, BiOCl has been produced firstly and transformed to the $BiOCl/Bi_2S_3$ composite by ion exchange in the presence of a suitable sulfur source [40,41].

Herein, we report one-pot, surfactant free, large scale and controlled synthesis of uniform and novel architectures of $BiOCl/Bi_2S_3$ hetero-structures through a facile solvothermal method. The hetero-structures exhibit significantly enhanced photo-catalytic activity compared with pure BiOCl, Bi_2S_3 and commercially available TiO_2 powder in the photo-degradation of MO aqueous solutions. A "bottom-up" assembly has been developed to synthesize well-defined architectures at a large scale.

EXPERIMENTAL SECTION

All chemical reagents used in this experiment were of analytical grade and have been used without further purification. The BiOCl, Bi_2S_3 and $BiOCl/Bi_2S_3$ hetero-structures were prepared by solvothermal method. In a representative procedure, 1 mmol of $BiCl_3$ was dissolved in 40 mL of ethanol and then 2 mmol of sulfur powder was added and stirred magnetically for 30 min to disperse all reagents homogeneously at room temperature. The resulting precursor suspension was transferred into a Teflon-lined stainless steel autoclave of 50 mL, maintained at 180°C for 8 h and subsequently cooled to room temperature. The product was collected after filtration, washed with distilled water, acetone and ethanol several times and dried at 80°C. In order to observe the growth mechanism, the same experiment was repeated at different temperatures, reaction durations, sulfur sources and solvents, while the precursor ratios and all other experimental conditions were unchanged.

The powder X-ray diffraction patterns (XRD) of the samples were recorded on Japan Rigaku D/max-rA equipped with graphite monochromatized high-intensity Cu-Kα radiation (λ=1.54178 Å). Chemical analysis was performed using energy dispersive X-ray spectrometry (EDS) by utilizing a JEOL JSM-6700F scanning electron microscope (SEM). X-ray photoelectron spectroscopy (XPS) valence spectra were acquired on an ESCALAB MKII X-ray photoelectron spectrometer with an excitation source of Mg Kα=1253.6 eV. The transmission electron microscopy (TEM) images were taken on the H-7650 (Hitachi, Japan) operated at an acceleration voltage of 100 kV. High resolution transmission electron microscopy (HRTEM) and the corresponding electron diffraction (ED) analyses were carried out by using a JEOL-2010 TEM at an acceleration voltage of 200 kV. Room-temperature UV-vis absorption spectroscopy was conducted on a Perkin Elmer Lambda 950 UV-vis-NIR spectrophotometer using an integrating sphere accessory.

Photocatalytic activities of the samples were evaluated by the degradation of MO aqueous solution under visible-light irradiation. A 300 W Xe lamp was used as the light source (λ>400 nm). In each experiment 20 mg of the photo-catalyst was added to the MO solution (200 mL, 25 mg L^{-1}). Before illumination, the suspensions were stirred for 60 min in the dark in order to reach an adsorption-desorption equilibrium between the photo-catalysts and the organic dyes. All the experiments were conducted in air at room temperature. At given time intervals about 3 mL of the suspensions were removed with a medical injector and monitored using a UV-vis spectrometer after centrifugation to remove the photo-catalyst particles.

Detection of hydroxyl radicals (•OH) was carried out using 20 mg of the catalyst with 50 mL of an aqueous solution of 3×10^{-3} mol L^{-1} terephthalic acid (TA) and 10×10^{-3} mol L^{-1} NaOH. This mixture was kept in the dark for 30 min under constant magnetic stirring before exposing to visible light irradiation (the same source was used for the visible light irradiation in the photocatalytic tests). 5 mL of the suspension was taken every 10 min and centrifuged before measuring the fluorescence. The photo-generated •OH radicals reacted with TA to form 2-hydroxyterephthalic acid (TAOH) and showed a typical fluorescence peak at 426 nm. A fluorescence spectrophotometer (Hitachi FL-4500) was employed to analyze the fluorescence spectra of the generated 2-hydroxyl terephthalic acid (TAOH). The excitation light with a wavelength of 320 nm was set during the measurements of the fluorescence signals. An increase in the fluorescence intensity is directly associated with an increase in

the amount of photogenerated ·OH radicals.

RESULTS AND DISCUSSION

Fig. 1 shows the X-ray diffraction patterns of the as-prepared BiOCl, Bi_2S_3 and BiOCl/Bi_2S_3 hetero-structure (C3). It is observed that all the peaks of Fig. 1a coincide with the standard diffraction of tetragonal BiOCl (JCPDS No. 06-0249), indicating the formation of pure BiOCl. In the presence of sulfur powder, the solution proceeded for 8 h under the same experimental condition, new peaks belonging to Bi_2S_3 appeared in the XRD pattern named C3 as shown in Fig. 1b. The coexistence of BiOCl and Bi_2S_3 peaks in the pattern of C3 indicates BiOCl/Bi_2S_3 hetero-structure. When reaction time proceeded up to 14 h, the diffraction peaks of BiOCl completely disappeared and all the peaks of the product are consistent with orthorhombic Bi_2S_3 (JCPDS No. 17-0320), as shown in Fig. 1c. The corresponding EDS patterns of BiOCl, C3 and Bi_2S_3 have been displayed in Fig. S1. The XRD patterns of all of the fabricated hetero-structures (C1–C5) have been shown in Fig. S2. With reaction time increasing, the intensities of Bi_2S_3 diffraction peaks increase whereas those of BiOCl decreased simultaneously, indicating that BiOCl transformed gradually into Bi_2S_3. To further detect the chemical compositions of BiOCl/Bi_2S_3 hetero-structures, XPS analysis (Fig. 2) of sample C3 was conducted. The typical XPS survey spectrum (Fig. 2a) shows that the hetero-structures are composed of Bi, O, Cl, and S elements. The additional C 1s peak can be ascribed to the adventitious hydrocarbon.

A SEM image of the BiOCl/Bi_2S_3 hetero-structure (C3) is illustrated in Fig. 3a–c. From Fig. 3a, b, it can be observed that the structure is produced at large scale and the micro-architectures are uniform in shape and size without agglomeration. From Fig. 3c, the hetero-structures like electronic chips (ECs) consist of a uniform micro plate at the center and rods like prongs stretching out from all edges of the plate. The surface of plate is smooth and have the edge length approximately 20 μm and the rod length within 15 μm. More detailed insights into the microstructure of the sample C3 are given by TEM, HRTEM and SAED investigations. Fig. S3a shows the TEM image of single ECs like micro structure, the plates and the rods have smooth surfaces. HRTEM images taken from the joint of plate and a prong of single hetero-structure are shown in Fig. 3d, where clear lattice fringes from the portion of a plate with d-spacing of 0.375 nm correspond to the (002) lattice plane of BiOCl in C3 sample, suggesting that the BiOCl plates to be well-crystallized. A corresponding SAED pattern conducted at this

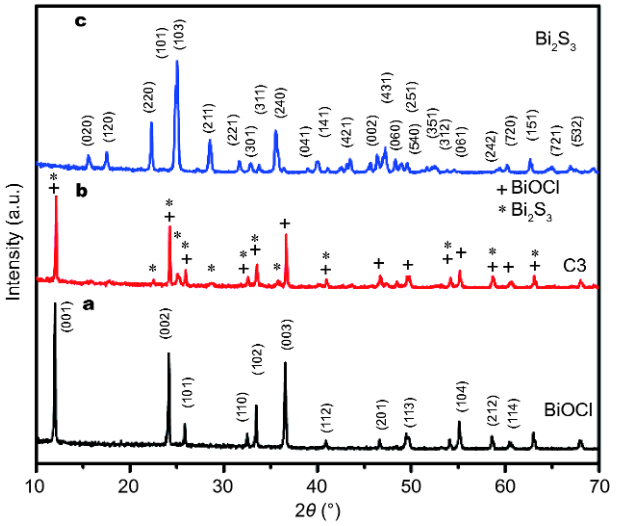

Figure 1 XRD patterns of (a) BiOCl precursor, (b) BiOCl/Bi_2S_3 hetero-structure (C3) and (c) Bi_2S_3.

portion of single ECs like hetero-structure (Fig. S3b) confirm its single crystal structure. And a typical HRTEM image taken from a rod-like prong portion as indicated in the Fig. 3d with well-resolved inter-planar d-spacing of 0.293 nm showed the (211) lattice plane of Bi_2S_3. The bright SAED pattern displayed within the inset of Fig. S3c indicated the well-defined and single crystalline feature of Bi_2S_3 within C3 composite. The SAED pattern indicates the joint portion of plate and rod (Fig. S3d) is polycrystalline. So within the single ECs microstructure the plate is entirely composed of single crystalline BiOCl and the rods are composed of single crystalline Bi_2S_3.

Fig. 4 displays the UV-vis absorption spectra of all the as-prepared samples. The white BiOCl only exhibits UV light response with an absorption edge around 380 nm, while the black Bi_2S_3 shows an intense absorption from the visible range to the infrared region. It is evident that the BiOCl/Bi_2S_3 hetero-structure composites show tunable visible light absorption in a large range.

With increasing Bi_2S_3 content, the absorption edge of BiOCl/Bi_2S_3 had a significant red shift compared to BiOCl. Based on the absorption spectra, the band gap energy (E_g) of the samples can be determined by the formula [42]:

$$\alpha h\upsilon = A\left(h\upsilon - E_g\right)^{n/2},$$

where α, υ, E_g and A are absorption coefficient, light frequency, band gap energy and a constant, respectively. Among them, n is determined by the type of optical transition of a semiconductor (n=1 for direct transition and n=4 for indirect transition). For BiOCl and Bi_2S_3, the

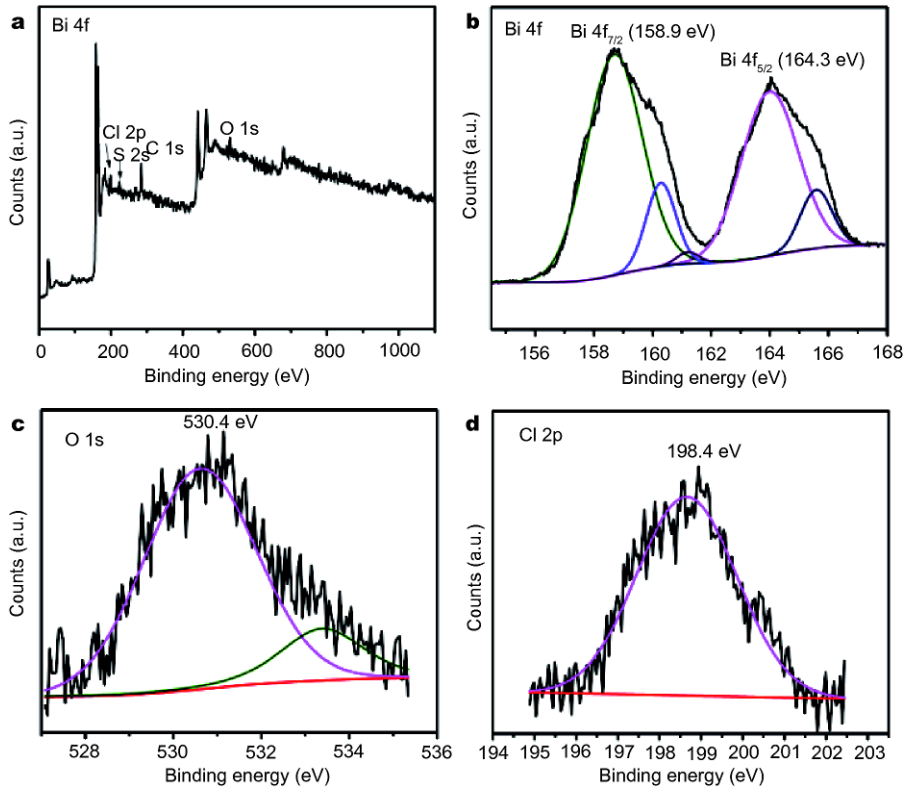

Figure 2 (a) XPS survey spectrum of a representative BiOCl/Bi_2S_3 hetero-structure (C3) and the corresponding high-resolution XPS spectra of Bi 4f (b), O 1s (c) and Cl 2p (d).

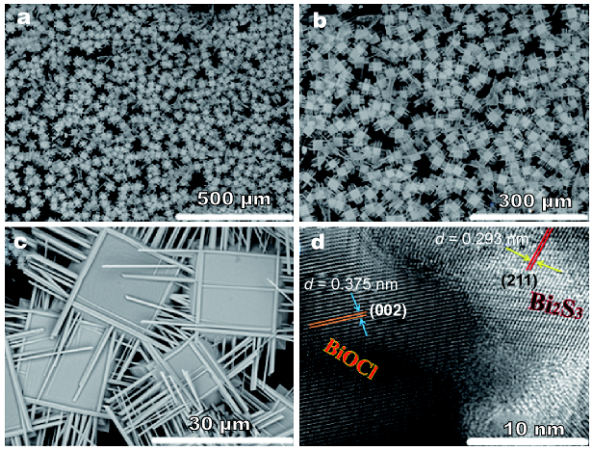

Figure 3 (a–c) SEM images of BiOCl/Bi_2S_3 hetero-structure (C3); (d) HRTEM image taken from the joint of plate and a prong of a single EC like particle of BiOCl/Bi_2S_3 hetero-structure (C3).

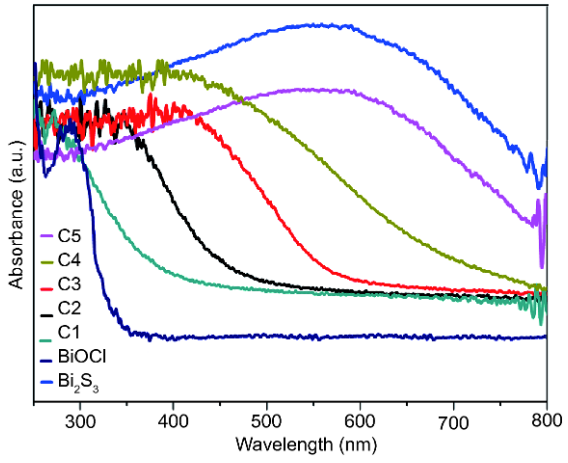

Figure 4 UV-vis absorption spectra of BiOCl precursor, BiOCl/Bi_2S_3 composites (C1, C2, C3, C4 and C5) and Bi_2S_3.

values of n are 4 and 1, respectively [41]. Thus, the E_g estimated from the intercept of the tangents to the plot of $(\alpha h\nu)^{1/2}$ versus $h\nu$ was 3.20 eV for BiOCl while the E_g from the plot of $(\alpha h\nu)^2$ versus $h\nu$ was 1.46 eV for Bi_2S_3 and 1.68, 2.0, 2.31, 2.81, 3.05 for C1, C2, C3, C4, C5 hetero-structure composites, respectively (Figs. S4, S5).

The photo-catalytic activities of the as-prepared hetero-structures composites were investigated by the degradation of MO dye aqueous solution under visible light irradiation (λ>400 nm). Fig. 5d shows the change of

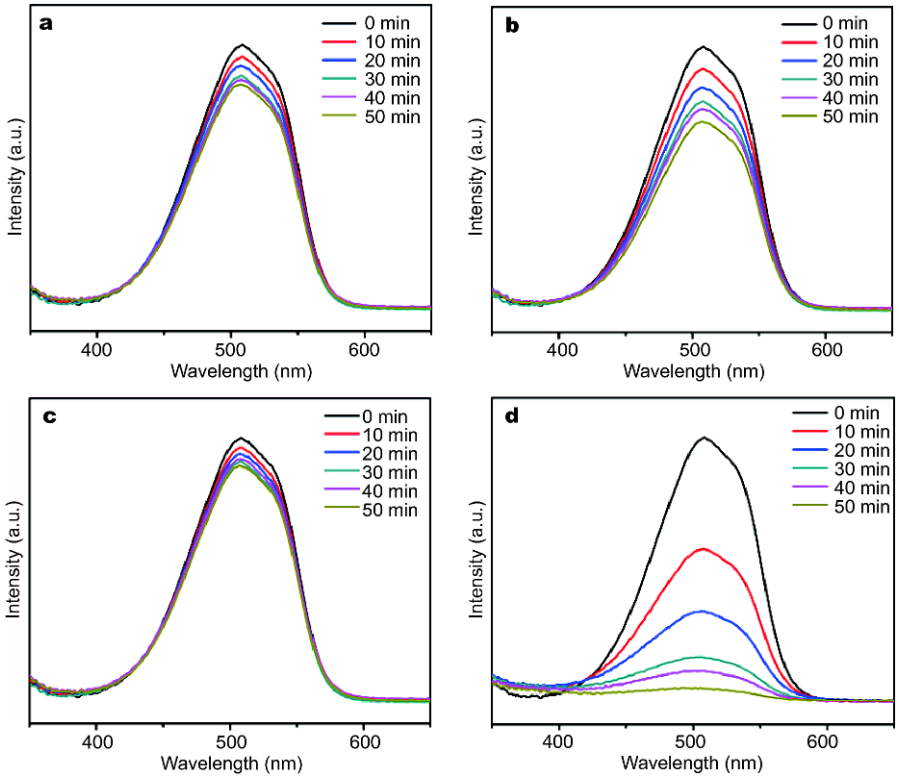

Figure 5 Absorption spectra of photo-degradation of MO aqueous solution by different catalysts (20 mg) within 50 min of visible light irradiation at room temperature Bi_2S_3 (a), BiOCl (b), P25 (c), BiOCl/Bi_2S_3 (d) hetero-structure (C3).

absorption spectra of MO solution exposed to visible light as a function of time in C3. With the increasing irradiation time, the peak intensity of MO at around 503 nm decreased gradually. But within the same time, the degradation capabilities of Bi_2S_3, BiOCl and even the TiO_2 commercially available powders were very low; as shown in Fig. 5a–c respectively. Under the same degradations, another hetero-structures (C1, C2, C4 and C5) have also been employed to degrade the MO dye (Fig. S6). The degradation efficiency of all the photo-catalysts has been shown in Fig. 6a. Fig. 6b shows the variation of MO concentration (C_0/C) with photo-degradation time over different photo-catalysts and Fig. 6c reveals that the rate constant k of all the BiOCl/Bi_2S_3 hetero-structure composites (C1–C5) are higher than single BiOCl and Bi_2S_3, confirming the higher photocatalytic activity of BiOCl/Bi_2S_3. Moreover, the as-synthesized C3 was recycled 6 times for the degradation of MO to ascertain their stability. The efficiency of C3 was 100% for the first time and for 2^{nd}, 3^{rd}, 4^{th}, 5^{th} and 6^{th} time, it has been evaluated to be 99.5%, 99%, 98.5%, 98% and 97%, respectively. So, just 3% decrease in the efficiency after the 6^{th} recycle describes a significant recycling capability of C3 with a slight reduction in catalytic activity (Fig. 6d). Overall, it has observed that all BiOCl/Bi_2S_3 heterostructures exhibit higher photocatalytic activity than single BiOCl and Bi_2S_3. The interface of the semi-conductor hetero-structures facilitates the separation of photo-induced carriers and then enhances the photo-catalytic activity.

Only three raw materials, bismuth chloride, sulfur powder and ethanol, were included in the reaction and these provide a simple surfactant free model system for investigating the reaction mechanism. In solvothermal treatment the ethanol solution acts not only as a common solvent, but also plays a key role as a reducing agent, as ethanol loses two electrons to form acetaldehyde, which is accompanied by the transfer of electrons to S to form H_2S. In order to thoroughly understand the formation mechanism of the novel electronic chips like architectures of BiOCl/Bi_2S_3 hetero-structure (C3) composite, the influence of the reaction temperature, reaction duration, different solvents and variety of sulfur sources on the formation of the novel hetero-structure was studied. Apart from being a reagent for the production of H_2S, sulfur powder also acted as original nuclei to initiate the formation of Bi_2S_3 [43]. The regular architectures could be

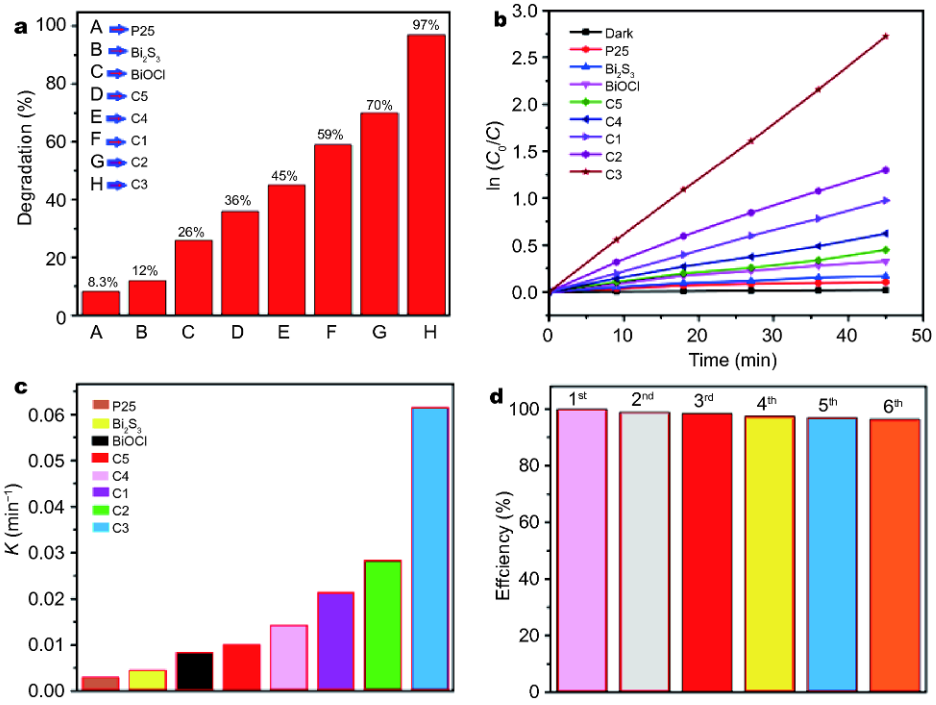

Figure 6 (a) A plot of the extent of photo-degradation of MO aqueous solution by different catalysts (20 mg) within 50 min of visible light irradiation at room temperature; (b) the MB normalization concentration (from the optical absorbance measurements at 504 nm) in the solution with different catalysts *vs*. the exposure time of the as prepared products and commercially available P25 powder; (c) first order rate constant K (min^{-1}) of the as prepared products and commercially available P25 powder; (d) stability test of as prepared BiOCl/Bi_2S_3 hetero-structure composite (C3) in degrading of MO aqueous solution for 6 repeated cycles.

formed only in sulfur powder and ethanol (Figs S7, S8). With an increase of temperature, the solubility of the S powder slightly increases and solid, tiny sulfur particles are melted and transformed into liquid droplets. We have investigated the effect of temperature on the morphology of the superstructures at different reaction temperatures (Fig. S9). With an increase in the reaction temperature, especially temperatures that exceed 120°C (the melting point of sulfur), the architectures with a defined shapes emerged. This may be due to the heating process making uniform S sphere droplets and reactive H_2S, simultaneously, which constructs the forthcoming structures, but beyond a certain temperature (180°C) the morphology was distorted. So, 180°C was found to be the most feasible temperature to synthesis the electronic chips like homogeneous architectures. We have monitored the growth process of the novel electronic chips like architectures at 180°C by stopping the reaction at different time intervals and observed the morphology by SEM (Fig. 7). This showed a shape evolution as the reaction time increases; the corresponding XRD spectra are shown in Fig. S2.

As shown in Fig. 7 and Fig. S10, at the initial stage of the reaction as the reaction was processed under typical

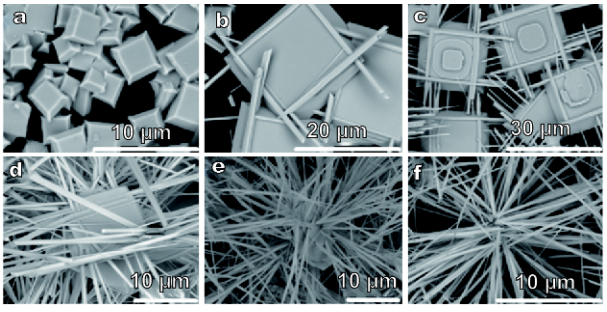

Figure 7 SEM images of the as-prepared products for different reaction durations, under the same typical experimental conditions (a) 2 h in the absence of sulfur powder, (b) 4 h (C1), (c) 6 h (C2), (d) 10 h (C4), (e) 12 h (C5), (f) 14 h (Bi_2S_3).

experimental conditions only for 4 h the square plate with prongs like rods (Fig. 7b) were observed. After 6 h, the prongs stretching from the plate also were doubled (Fig. 7c). More increment in the reaction duration and preceding the reaction up to 8 h resulted in well-defined rods from all the four edges of the plate, as shown in Fig. 3 in the form of ECs (C3) were observed at large scale. The reaction duration up to 10 h caused the emergence of the rods with the increased length and size from all sides of

the plate (Fig. 7d). When the reaction was extended to 12 h (Fig. 7e), the size of rods was much increased and the dimension of the plate was extremely decreased, even the plates were hard to find. Finally when the reaction was extended to 14 h, the plates completely disappeared (Fig. 7f). XRD and EDS spectra confirmed the obtained rod bunches are single crystal Bi_2S_3. Under the same experimental procedure, as we observed, in the absence of sulfur powder, the product (Fig. 7a) only consist of plates and the corresponding XRD and EDS spectra confirmed the product to be the single crystal BiOCl.

On the basis of the above experimental results, it can be inferred that BiOCl plates are formed firstly from the hydrolysis of $BiCl_3$ due to the traces of water in the absolute ethanol (Equation (1)) [44]. The plate-like morphology comes from the layered structure of single crystal BiOCl, which is constructed by the combination of the metal oxygen Bi_2O^{2+} layer and double the chloride ion layers. The bonding within the layers is strong and primarily covalent, whereas the interaction between the layers is a van der Waals force. In addition, it has been reported that ethanol would reduce Sb_2O_3 to Sb. It can be conjectured here that, most probably, BiOCl can be reduced to active Bi by ethanol at 180 °C under the present conditions (Equation (2)). Thus the newly active Bi atoms can easily combine the S atoms to Bi_2S_3 (Equation (3)) and the reaction process is described within these equations collectively, as follows [44]:

$$BiCl_3 + H_2O \rightarrow BiOCl + HCl, \quad (1)$$

$$BiOCl + CH_3CH_2OH \rightarrow Bi + CH_3CHO + HCl + H_2O, \quad (2)$$

$$Bi + S \rightarrow Bi_2S_3. \quad (3)$$

So Bi_2S_3 prongs are formed spontaneously on the surface of BiOCl plates. Since, Bi_2S_3 has a much smaller solubility than BiOCl, the latter is unstable in this reaction. The preferential growth of Bi_2S_3 into nanorods/microwires depends on its intrinsic nature. Bi_2S_3 is a highly anisotropic semi-conductor with layered structure parallel to the growth direction [35], so the composite BiOCl/Bi_2S_3 has the Bi_2S_3 prongs and BiOCl plate with increasing reaction duration. The corresponding XRD pattern only shows the strong peaks of BiOCl in the absence of S powder, while sample C1 shows some peaks of Bi_2S_3. The composite BiOCl/Bi_2S_3 is formed finally after the reaction duration of 14 h. The whole process has been schematically illustrated in Fig. 8. The electronic chips like BiOCl/Bi_2S_3 hetero-structures through chemical BiOCl plates is formed through Kirkendall effect [45]. It has been proposed that the core-shell Bi_2S_3 microspheres were produced by the chemical transformation of the BiOCl microspheres. Accordingly, a mechanism for the formation of the electronic chips like BiOCl/Bi_2S_3 hetero-structures and the rod bunches like Bi_2S_3 microstructures is proposed. First, BiOCl plates are formed, and subsequently, while S^{2-} ions originate from the sulfur source within the reaction. A layer of interconnected network consisting of primary Bi_2S_3 particles was formed around the exterior surface of the BiOCl plates as long as they were surrounded by the reactant S^{2-} ions with an adequate concentration. Then the network developed due to the coupled reaction-diffusion process. The formation of final Bi_2S_3 structure depended on the inward S^{2-} ion diffusion rate relative to the outward Bi^{3+} ion diffusion rate and the composite BiOCl/Bi_2S_3 structures could result from the much higher inward diffusion rate of the S^{2-} ions and continue to the complete chemical transformation of BiOCl to Bi_2S_3 with the continuous increment of reaction duration, similar to the reported formation of Ag rhombdodecahedral microparticles [45,46].

Under the irradiation of visible light, the electron-hole pairs are produced and a series of photo-induced reactive species, including h^+, $^{\bullet}OH$ or $^{\bullet}O^{2-}$, directly take part in the photo-catalytic oxidation process [47,48], as shown in Equations 4–7. According to the earlier report [41], h^+ and $^{\bullet}O^{2-}$ played a more important role than $^{\bullet}OH$ in the photo-degradation of organic dyes. Dissolved oxygen acts as an efficient electrons trap responsible for the direct generation of $^{\bullet}O^{2-}$ over BiOCl/Bi_2S_3 hetero-structure system.

$$\text{Catalyst} + h\nu \rightarrow e^- + h^+, \quad (4)$$

$$2e^- + O_2 \rightarrow O^- + 2h^+, \quad (5)$$

$$2e^- + O^{-2} + 2H^+ \rightarrow {}^{\bullet}OH + OH^-, \quad (6)$$

$$RhB + {}^{\bullet}O^{-2}(h^+, {}^{\bullet}OH) \rightarrow \text{products}. \quad (7)$$

Then the carriers transfer to the catalyst surface to react with the adsorbed reactants and the migration direction of the photo-generated charge carriers is dependent on the relative band edge positions of the two components in composite photo-catalysts [49].

Based on the band gap structure of BiOCl/Bi_2S_3 hetero-structure composite, a possible enhancement mechanism

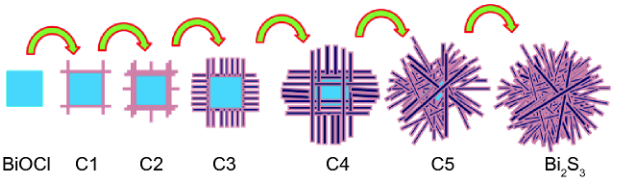

Figure 8 Growth mechanism; starting from BiOCl and formation of BiOCl/Bi_2S_3 hetero-structure composites then transformation into Bi_2S_3.

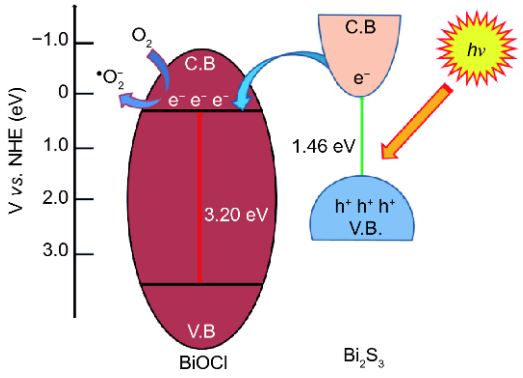

Figure 9 Schematic illustration of the charge transfer and the possible reaction mechanism of BiOCl/Bi_2S_3 hetero-structure under visible light irradiation.

for the photo-catalyst activity of BiOCl/Bi_2S_3 hetero-structure photo-catalyst is proposed (Fig. 9). Under visible-light (λ>400 nm), Bi_2S_3 with narrow E_g will be activated while BiOCl with large E_g will be not. The electrons on the conduction band (CB) of Bi_2S_3 could migrate easily to the valence band (VB) of BiOCl and then react with O_2 adsorbed on the surface of BiOCl/Bi_2S_3 to produce $^{\bullet}O^{2-}$, further decomposing MO. In addition, the holes stayed on the VB of Bi_2S_3 would degrade MO directly because the VB potential of Bi_2S_3 is more negative than the standard reduction potential of $H_2O/^{\bullet}OH$, H^+ (2.72 eV) [41]. Thus the recombination rate of photo-generated electrons and holes was decreased largely. The BiOCl/Bi_2S_3 hetero-structures exhibit more excellent photo-catalytic properties than those of single Bi_2S_3, BiOCl and commercially available P25 powder.

Besides the above described reasons, proving the superior photocatalytic degradation of BiOCl/Bi_2S_3 hetero-structure composite (C3), it is also worth estimating the amount of active species taking part in the photocatalytic reaction. Since, during the photo-oxidation reaction, the photo-induced holes in the VB react with surface-adsorbed water to produce hydroxyl radicals ($^{\bullet}OH$) [50]. That is why, the photo-generated holes or the formed $^{\bullet}OH$ radicals are considered as the two-main species to oxidize the organic dyes in the aqueous solution [50]. During the radical detection experiments, it has been seen that, the $^{\bullet}OH$ radicals react with TA to form 2-hydroxyl terephthalic acid (TAOH), which exhibits a characteristic fluorescence peak around 426 nm (Fig. 10) and is used as indirect evidence to monitor the amount of $^{\bullet}OH$ radicals [51]. For each experiment, the fluorescence peak gradually increases with an increase in irradiation

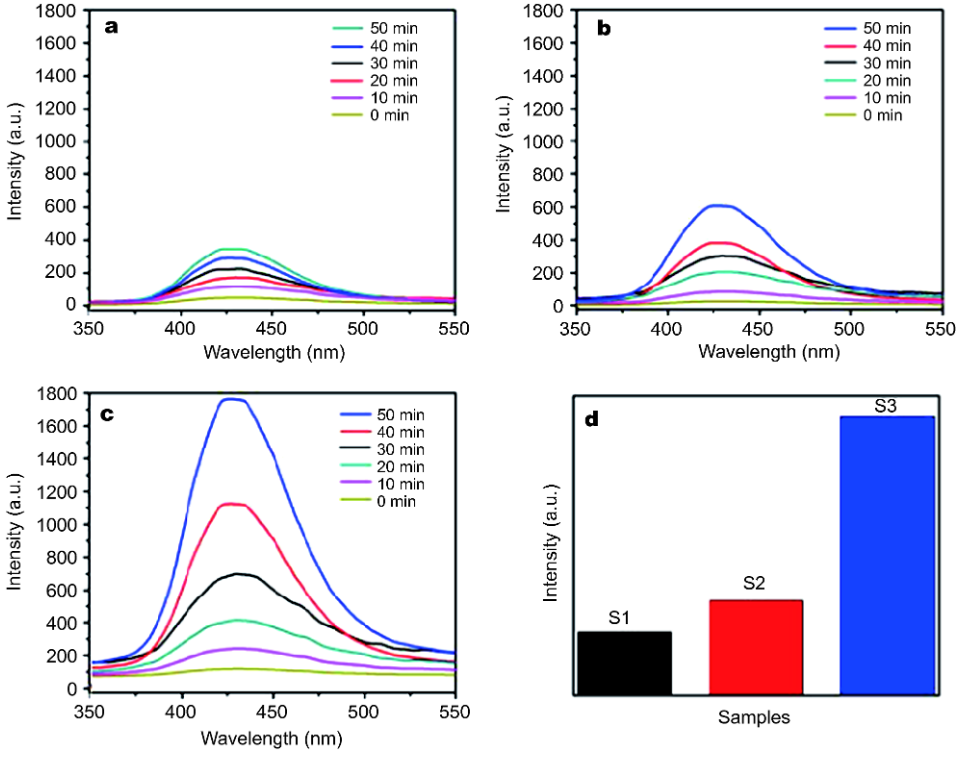

Figure 10 Fluorescence spectra of 2-hydroxyl terephthalic acid (TAOH) solution generated by Bi_2S_3 (a), BiOCl (b), BiOCl/Bi_2S_3 (c), hetero-structure composite (C3) for 50 min, and (d) comparison of the amount of final TAOH generated after 50 min from (a) to (c).

time which is evidence of the formation of hydroxyl radicals. Fig. 10a, b shows that a few $^{\bullet}OH$ radicals formed in 50 min for the case of the as synthesized singlet Bi_2S_3 and BiOCl, hence it took a longer time to decompose the dye which is in good agreement with the photocatalytic activity of single Bi_2S_3 and BiOCl (Fig. 6). From Fig. 10c, it can be examined that the maximum $^{\bullet}OH$ radicals were formed when the BiOCl/Bi_2S_3 hetero-structure composite (C3) was used in the TAOH solution (Fig. 10c), suggesting the excellent capability of BiOCl/Bi_2S_3 hetero-structure composite (C3) for decomposing MO. Fig. 10d indicates the comparison of the amount of TAOH generated after an irradiation of 50 min regarding each of the three as synthesized photocatalytic samples.

CONCLUSIONS

In summary, we have successfully fabricated uniform and BiOCl/Bi_2S_3 hetero-structures through a solvothermal route. The hetero-structures were evaluated as photocatalysts for the degradation of MO under visible light irradiation. It has been found that photo-catalytic efficiency of the BiOCl/Bi_2S_3 hetero-structures is significantly enhanced, attributed to the efficient separation of the recombination of electron-hole pairs. Furthermore, these atypical architectures were simply synthesized using inexpensive precursors through a facile template-free method which gives a great promise for large scale production without further treatment to remove the template *via* strong acids. The morphology of the ECs-like BiOCl/Bi_2S_3 hetero-structures can easily be tailored by making a slight change in the mentioned procedure that emphasizes the generalization of the devised synthesis method. Overall, the study is quite helpful for the design of new, unique, atypical and homogeneous photo-catalysts with enhanced photo-catalytic performances within the visible range of light.

Received 21 June 2017; accepted 3 October 2017; published online 27 November 2017

1 Tahir M, Mahmood N, Zhu J, *et al.* One dimensional graphitic carbon nitrides as effective metal-free oxygen reduction catalysts. Sci Rep, 2015, 5: 12389
2 Tahir M, Cao C, Butt FK, *et al.* Tubular graphitic-C_3N_4: a prospective material for energy storage and green photocatalysis. J Mater Chem A, 2013, 1: 13949–13955
3 Tahir M, Cao C, Mahmood N, *et al.* Multifunctional g-C_3N_4 nanofibers: a template-free fabrication and enhanced optical, electrochemical, and photocatalyst properties. ACS Appl Mater Interfaces, 2014, 6: 1258–1265
4 Wu Y, Cao C, Zhu Y, *et al.* Cube-shaped hierarchical $LiNi_{1/3}Co_{1/3}Mn_{1/3}O_2$ with enhanced growth of nanocrystal planes as high-performance cathode materials for lithium-ion batteries. J Mater Chem A, 2015, 3: 15523–15528
5 Meng R, Jiang J, Liang Q, *et al.* Design of graphene-like gallium nitride and WS_2/WSe_2 nanocomposites for photocatalyst applications. Sci China Mater, 2016, 59: 1027–1036
6 Wu Y, Zhang J, Cao C. Scalable and general synthesis of spinel manganese-based cathodes with hierarchical yolk-shell structure and superior lithium storage properties. Nano Res, 2017, doi 10.1007/s12274-017-1625-0
7 Lu X, Li Y, Bai X, *et al.* Multifunctional $Cu_{1.94}S$-Bi_2S_3@polymer nanocomposites for computed tomography imaging guided photothermal ablation. Sci China Mater, 2017, 60: 777–788
8 Liu H, Ma H, Joo J, *et al.* Contribution of multiple reflections to light utilization efficiency of submicron hollow TiO_2 photocatalyst. Sci China Mater, 2016, 59: 1017–1026
9 Xi G, Yue B, Cao J, *et al.* Fe_3O_4/WO_3 hierarchical core-shell structure: high-performance and recyclable visible-light photocatalysis. Chem Eur J, 2011, 17: 5145–5154
10 Xi G, Ye J. Synthesis of bismuth vanadate nanoplates with exposed {001} facets and enhanced visible-light photocatalytic properties. Chem Commun, 2010, 46: 1893–1895
11 Liang Q, Li Z, Bai Y, *et al.* Reduced-sized monolayer carbon nitride nanosheets for highly improved photoresponse for cell imaging and photocatalysis. Sci China Mater, 2017, 60: 109–118
12 Wu Y, Cao C, Zhang J, *et al.* Hierarchical $LiMn_2O_4$ hollow cubes with exposed {111} planes as high-power cathodes for lithium-ion batteries. ACS Appl Mater Interfaces, 2016, 8: 19567–19572
13 Chen Y, Tian G, Guo Q, *et al.* One-step synthesis of a hierarchical Bi_2S_3nanoflower\In_2S_3 nanosheet composite with efficient visible-light photocatalytic activity. CrystEngComm, 2015, 17: 8720–8727
14 Shi Y, Chen Y, Tian G, *et al.* One-pot controlled synthesis of sea-urchin shaped Bi_2S_3/CdS hierarchical heterostructures with excellent visible light photocatalytic activity. Dalton Trans, 2014, 43: 12396–12404
15 Zhou J, Tian G, Chen Y, *et al.* Growth rate controlled synthesis of hierarchical Bi_2S_3/In_2S_3 core/shell microspheres with enhanced photocatalytic activity. Sci Rep, 2015, 4: 4027
16 Tahir M, Mahmood N, Zhang X, *et al.* Bifunctional catalysts of Co_3O_4@GCN tubular nanostructured (TNS) hybrids for oxygen and hydrogen evolution reactions. Nano Res, 2015, 8: 3725–3736
17 Tanveer M, Cao C, Ali Z, *et al.* Template free synthesis of CuS nanosheet-based hierarchical microspheres: an efficient natural light driven photocatalyst. CrystEngComm, 2014, 16: 5290–5300
18 Tanveer M, Cao C, Aslam I, *et al.* Effect of the morphology of CuS upon the photocatalytic degradation of organic dyes. RSC Adv, 2014, 4: 63447–63456
19 Ali Z, Cao C, Li J, *et al.* Effect of synthesis technique on electrochemical performance of bismuth selenide. J Power Sources, 2013, 229: 216–222
20 Ali Z, Mirza M, Cao C, *et al.* Wide range photodetector based on catalyst free grown indium selenide microwires. ACS Appl Mater Interfaces, 2014, 6: 9550–9556
21 Aslam I, Cao C, Tanveer M, *et al.* A novel Z-scheme WO_3/$CdWO_4$ photocatalyst with enhanced visible-light photocatalytic activity for the degradation of organic pollutants. RSC Adv, 2015, 5: 6019–6026
22 Aslam I, Cao C, Tanveer M, *et al.* A facile one-step fabrication of novel WO_3/$Fe_2(WO_4)_3$·10.7H_2O porous microplates with remarkable photocatalytic activities. CrystEngComm, 2015, 17: 4809–4817
23 Khalid S, Cao C, Wang L, *et al.* Microwave assisted synthesis of porous $NiCo_2O_4$ microspheres: application as high performance

asymmetric and symmetric supercapacitors with large areal capacitance. Sci Rep, 2016, 6: 22699
24 Hou J, Cao C, Idrees F, *et al.* Hierarchical porous nitrogen-doped carbon nanosheets derived from silk for ultrahigh-capacity battery anodes and supercapacitors. ACS Nano, 2015, 9: 2556–2564
25 Hou J, Cao C, Ma X, *et al.* From rice bran to high energy density supercapacitors: a new route to control porous structure of 3D carbon. Sci Rep, 2015, 4: 7260
26 Fujishima A, Honda K. Electrochemical photolysis of water at a semiconductor electrode. Nature, 1972, 238: 37–38
27 Zhang T, Oyama T, Horikoshi S, *et al.* Photocatalytic decomposition of the sodium dodecylbenzene sulfonate surfactant in aqueous titania suspensions exposed to highly concentrated solar radiation and effects of additives. Appl Catal B-Environ, 2003, 42: 13–24
28 Spadavecchia F, Cappelletti G, Ardizzone S, *et al.* Solar photoactivity of nano-N-TiO_2 from tertiary amine: role of defects and paramagnetic species. Appl Catal B-Environ, 2010, 96: 314–322
29 Sun WT, Yu Y, Pan HY, *et al.* CdS quantum dots sensitized TiO_2 nanotube-array photoelectrodes. J Am Chem Soc, 2008, 130: 1124–1125
30 Zhang LW, Wang YJ, Cheng HY, *et al.* Synthesis of porous Bi_2WO_6 thin films as efficient visible-light-active photocatalysts. Adv Mater, 2009, 21: 1286–1290
31 Xia J, Yin S, Li H, *et al.* Self-assembly and enhanced photocatalytic properties of BiOI hollow microspheres *via* a reactable ionic liquid. Langmuir, 2011, 27: 1200–1206
32 Zheng C, Cao C, Ali Z. *In situ* formed Bi/$BiOBr_xI_{1-x}$ heterojunction of hierarchical microspheres for efficient visible-light photocatalytic activity. Phys Chem Chem Phys, 2015, 17: 13347–13354
33 Xia J, Yin S, Li H, *et al.* Improved visible light photocatalytic activity of sphere-like BiOBr hollow and porous structures synthesized *via* a reactable ionic liquid. Dalton Trans, 2011, 40: 5249
34 Lv J, Kako T, Li Z, *et al.* Synthesis and photocatalytic activities of $NaNbO_3$ rods modified by In_2O_3 nanoparticles. J Phys Chem C, 2010, 114: 6157–6162
35 Dunkle SS, Helmich RJ, Suslick KS. $BiVO_4$ as a visible-light photocatalyst prepared by ultrasonic spray pyrolysis. J Phys Chem C, 2009, 113: 11980–11983
36 Henle J, Simon P, Frenzel A, *et al.* Nanosized BiOX (X=Cl, Br, I) particles synthesized in reverse microemulsions. Chem Mater, 2007, 19: 366–373
37 Zhang X, Ai Z, Jia F, *et al.* Generalized one-pot synthesis, characterization, and photocatalytic activity of hierarchical BiOX (X=Cl, Br, I) nanoplate microspheres. J Phys Chem C, 2008, 112: 747–753
38 Chang X, Yu G, Huang J, *et al.* Enhancement of photocatalytic activity over $NaBiO_3$/BiOCl composite prepared by an *in situ* formation strategy. Catal Today, 2010, 153: 193–199
39 Gao F, Zeng D, Huang Q, *et al.* Chemically bonded graphene/BiOCl nanocomposites as high-performance photocatalysts. Phys Chem Chem Phys, 2012, 14: 10572
40 Cheng H, Huang B, Qin X, *et al.* A controlled anion exchange strategy to synthesize Bi_2S_3 nanocrystals/BiOCl hybrid architectures with efficient visible light photoactivity. Chem Commun, 2012, 48: 97–99
41 Cao J, Xu B, Lin H, *et al.* Novel Bi_2S_3-sensitized BiOCl with highly visible light photocatalytic activity for the removal of rhodamine B. Catal Commun, 2012, 26: 204–208
42 Butler MA. Photoelectrolysis and physical properties of the semiconducting electrode WO_2. J Appl Phys, 1977, 48: 1914–1920
43 Zheng L, Xu Y, Song Y, *et al.* Nearly monodisperse $CuInS_2$ hierarchical microarchitectures for photocatalytic H_2 evolution under visible light. Inorg Chem, 2009, 48: 4003–4009
44 Zhu L, Xie Y, Zheng X, *et al.* Growth of compound Bi^{III}-VI^{A}-VII^{A} crystals with special morphologies under mild conditions. Inorg Chem, 2002, 41: 4560–4566
45 Yang J, Qi L, Lu C, *et al.* Morphosynthesis of rhombododecahedral silver cages by self-assembly coupled with precursor crystal templating. Angew Chem Int Ed, 2005, 44: 598–603
46 Li L, Cao R, Wang Z, *et al.* Template synthesis of hierarchical Bi_2E_3 (E=S, Se, Te) core-shell microspheres and their electrochemical and photoresponsive properties. J Phys Chem C, 2009, 113: 18075–18081
47 Zhou X, Hu C, Hu X, *et al.* Plasmon-assisted degradation of toxic pollutants with Ag-AgBr/Al_2O_3 under visible-light irradiation. J Phys Chem C, 2010, 114: 2746–2750
48 Yang Y, Zhang G, Yu S, *et al.* Efficient removal of organic contaminants by a visible light driven photocatalyst $Sr_6Bi_2O_9$. Chem Eng J, 2010, 162: 171–177
49 Madhusudan P, Ran J, Zhang J, *et al.* Novel urea assisted hydrothermal synthesis of hierarchical $BiVO_4$/$Bi_2O_2CO_3$ nanocomposites with enhanced visible-light photocatalytic activity. Appl Catal B-Environ, 2011, 110: 286–295
50 Linsebigler AL, Lu G, Yates JT. Photocatalysis on TiO_2 surfaces: principles, mechanisms, and selected results. Chem Rev, 1995, 95: 735–758
51 Hirakawa T, Nosaka Y. Properties of $O_2^{\cdot-}$ and $OH^{\cdot}$ formed in TiO_2 aqueous suspensions by photocatalytic reaction and the influence of H_2O_2 and some ions. Langmuir, 2002, 18: 3247–3254

Acknowledgements This work was supported by the National Natural Science Foundation of China (21371023), and the National Key Basic Research Program of China (2015CB251100).

Author contributions Tanveer M synthesized and modified all samples, performed all materials characterization and data analysis, and wrote this manuscript; Wu Y revised this manuscript; Cao C provided suggestions, helped interpret experimental results, and assisted in the preparation and revision of this manuscript. All authors contributed to the general dissicussion.

Conflict of interest The authors declare that they have no conflict of interest.

Supplementary information Experimental details are available in the online version of the paper.

Muhammad Tanveer obtained his MSc degree in solid state physics in 2009 from the University of the Punjab, Lahore, Pakistan. Later in 2011, he joined Beijing Institute of Technology (BIT), China and completed his PhD degree in materials physics and chemistry under the supervision of Prof. Chuanbao Cao. Currently, he is an assistant professor in the University of the Punjab, Lahore, Pakistan and the University of Lahore (UOL), Gujrat Campus, Gujrat, Pakistan. His research is focused on the fabrication of novel, unusual and atypical nano/micro architectures for energy harvesting and versatile applications.

Chuanbao Cao is currently the chief responsible professor of the School of Materials Science and Engineering, Director of Research Center of Materials Science of Beijing Institute of Technology (BIT), China. His research is focused on the electrochemical energy storage and conversion including electrode materials oflithium ion battery, super-capacitors and photo-electrochemical materials. Until now, he has published more than 300 peer-review research papers, holds or has filed 50 patents and patent applications.

具有显著光催化响应的非典型BiOCl/Bi_2S_3异质结构

Muhammad Tanveer[1,2,3], 吴宇[1], Muhammad Abdul Qadeer[4], 曹传宝[1*]

摘要 本文首次合成了具有独特形貌的异质结构BiOCl/Bi_2S_3. 相对于单一的BiOCl和Bi_2S_3, BiOCl/Bi_2S_3异质结构能有效地分离光生电子-空穴对以及抑制它们的再结合, 从而表现出更好的光催化降解甲基橙性能.

